The Abdus Salam International Centre for Theoretical Physics

United Nations Educational, Scientific and Cultural Organization

IAEA International Atomic Energy Agency

Spring College on the Physics of Complex Systems | (SMR 3817)

20 Feb 2023 - 17 Mar 2023
ICTP, Trieste, Italy

P01 - ACHARYA Anish

Conditional and stochastic resetting in a 1 d quantum system

P02 - GHOLIZADEH Sanaz

Multiplex network modeling for the impact of the opinion and behavior of mask wearing on the spreading and control of COVID-19

P03 - MAXWELL Julian

Interactions between life stages counteract positive population-level effects of mortality

P04 - MOAZZEN Najmeh

Prediction of Parkinson's disease using machine learning

P05 - RIVERA Nicole

Measuring climate teleconnections in Colombia through information transfer in a complex network.

P06 - ROBIGLIO Thomas

Simplicially driven simple contagion

P07 - WATWANI Jigyasa

Physics of Growth Regulation in Cells and TIssues

P01

Conditional and stochastic resetting in a 1 d quantum system

Stochastic resetting is a highly discussed topic in the statistical physics community these days and several non-trivial phenomena arise for different resetting or renewal protocols. I am interested in using this resetting process in a one-dimensional lattice system with a conditional resetting scheme. In this way, the system exhibits some non-trivial stationary state owing to this particular stochastic modulation. Currently, I am working on this project and I am solving this both analytically and numerically. My goal is to study the time dynamics of probability amplitude in lattice sites and observe other aspects using the said protocol. This technique helps study resetting processes with non-unitary evolution in quantum systems and investigates some appearance of stationary states at longer times. Moreover, the used approach is quite general, in a sense, it is independent of the Hamiltonian of the system under consideration. The scheme can be visualised as modelling environmental interactions or disturbances due to measurement apparatus. It also suffices the random nature of this kind of disturbance.

P02

Multiplex network modeling for the impact of the opinion and behavior of mask wearing on the spreading and control of COVID-19

We propose a network model to find out how and to what extent the level of people's opinions and behavior will affect the spread and transmission of a disease spreading such as the SEAIRS model of COVID-19. We have shown how two simultaneous spreading processes such as disease spreading and behavior-changing spreading work together and affect each other in the same group of the population by applying a multiplex network. Firstly we present a two-layer multiplex network for two spreading processes at the same time, one layer for disease spreading and the other for the dynamic of opinion behavior-changing toward mask-wearing as a protection measure for Covid 19 transmission. Then we apply a discrete Micro Markov Chain approach to express the dynamical system of the model. As well as the Markov chain, the threshold model exhibits people's behavior-changing parameters. We have investigated the effect of “peer pressure” and "fear of the increasing number of daily confirmed cases" on people’s behavior changes. Our results show that different levels of people's adherence to mask-wearing protection measures can influence disease spreading and vice-versa. Keywords: Covid19 transmission; multiplex network; mask-wearing behavior; mathematical model; Markov chain; threshold model

P03

Interactions between life stages counteract positive population-level effects of mortality

For an unstructured population model, meaning a model for the dynamics of indistinguishable individuals that accounts for population abundances only, conditions can be selected for the decreasing density-mortality rule to hold. This rule indicates that an increase in per-capita mortality leads to a decrease in population density at equilibrium. Under the same conditions, except now structure considered into the model, taking into account differences between individuals in age or size, this rule loses generality. The phenomenon of a population increasing in response to an increase in its per-capita mortality rate has been termed the "hydra effect". We evaluated the hydra effect in a resource-consumer structured population model (system of ODEs). Resources were kept unstructured. The model includes foraging, assimilation (including production of new juvenile offspring and maturation) and aging, and is stage-structured based on age: juveniles, adults, and post-reproductive adults. An increased mortality rate in post-reproductive individuals is considered, and its impact over the total population size in equilibrium is calculated. We found conditions leading to hydra effect and to anti-hydra effect. Interestingly, we found that adding a cooperation interaction (analog to commensalism between species) between post-reproductive and juvenile individuals counteracts the hydra effect, removing positive population-level effects of mortality. "Social populations", whose individuals interact cooperatively, respond negatively to an increase in old-age-related diseases, decreasing the steady state total population density. Since an empirical correlation has been found between found between the social character of mammal populations and lifespan of its individuals, these results may have implications in evolutionary biology.

P04

Prediction of Parkinson's disease using machine learning

Parkinson disease(PD), the second most common neurological disorder that causes significant disability, reduces the quality of life and has no cure. Nerve cells in this part of the brain are responsible for producing a chemical called dopamine. Dopamine acts as a message between the parts of the brain and nervous system that help control and co-ordinate body movements. As dopamine generally neurons in the parts begin to experience difficulty in speaking, writing, walking or completing other simple task .Approximately, 90% affected people with Parkinson have speech disorders. The average age of onset is about 70 years, and the incidence rises significantly with advancing age. However, a small percent of people with PD have “early-onset” disease that begins before the age of 50.More than 10 million people worldwide are living with PD. No cure for PD exists today, but research is ongoing and medications or surgery can often provide substantial improvement with motor symptoms. Parkinson disease is one of the most serious diseases. Hence diagnosing it at an earlier stage could help prevent or reduce the effects. The machine learning classification algorithms are used to predict if a person has Parkinson disease or not, comparing different machine learning algorithm such as logistic regression, decision tree, k-nearest neighbour as well as some “Ensemble” learning techniques where we attempt to improve the accuracy by combining several models .The machine learning model can be implemented to significantly improve diagnosis method of Parkinson disease.

P05

Measuring climate teleconnections in Colombia through information transfer in a complex network.

Climate is a complex system whose dynamics evolve on different spatio-temporal scales. It is impossible to predict from a mechanistic perspective given the number of variables and interactions to which it is subject. In the study of climate variability, one of the alternative approaches to classical modeling consists of the design of complex networks constructed from metrics derived from measurable physical quantities or statistical relationships. Recently, Liang and Kleeman proposed a theoretical formalism to measure information transfer -based on mutual entropies- between time series of variables that are dynamically related. This rate of information transfer measures the causal relationship between the variables, the direction of causality and how one variable influences the predictability of the other. In this work we use the Liang-Kleeman formalism to estimate and analyze the causal relationships between geographical areas more than 1000 km apart, in order to establish possible climatic teleconnections in a region of northern South America that includes the Colombian territory. We constructed a complex network whose nodes correspond to a regular division of the surface of the study area and its links are defined by the transfer of information from global climatic phenomena -such as ElNino3.4 - to the climatic variables. We include monthly data of surface temperature, pressure, humidity and climate variability indices for the period 1970-2020. Our results show a high connectivity of the Colombian territory with global climatic processes. Likewise, the influence of oceanic processes in the links established throughout the study area is verified.

P06

Simplicially driven simple contagion

Maxime Lucas,[1,2,*] Iacopo Iacopini,[3,*] Thomas Robiglio,[4] Alain Barrat,[5,†] and Giovanni Petri[1,2,†]

[1]*Mathematics and Complex Systems Research Area, ISI Foundation, Via Chisola 5, 10126 Turin, Italy*
[2]*CENTAI, Corso Inghilterra 3, Turin, Italy*
[3]*Department of Network and Data Science, Central European University, 1100 Vienna, Austria*
[4]*Department of Physics, University of Turin, Via Pietro Giuria 1, 10125 Turin, Italy*
[5]*Aix Marseille Univ, Université de Toulon, CNRS, CPT, Marseille, 13009, France*

(Dated: June 16, 2022)

Single contagion processes are known to display a continuous transition from an epidemic-free phase at low contagion rates to the epidemic state for rates above a critical threshold. This transition can become discontinuous when two simple contagion processes are coupled in a bi-directional symmetric way. However, in many cases, the coupling is not symmetric and the processes can be of a different nature. For example, social behaviors—such as hand-washing or mask-wearing—can affect the spread of a disease, and their adoption dynamics via social reinforcement mechanisms are better described by complex contagion models, rather than by the simple contagion paradigm, which is more appropriate for disease spreading phenomena. Motivated by this example, we consider a simplicial contagion (describing the adoption of a behavior) that uni-directionally drives a simple contagion (describing a disease propagation). We show that, above a critical driving strength, such driven simple contagion can exhibit both discontinuous transitions and bi-stability, which are instead absent in standard simple contagions. We provide a mean-field analytical description of the phase diagram of the system, and complement the results with Markov-chain simulations. Our results provide a novel route for a simple contagion process to display the phenomenology of a higher-order contagion, through a driving mechanism that may be hidden or unobservable in many practical instances.

Contagion processes have been widely studied using complex networks as the underlying structure supporting the propagation [1–3]: dynamical processes such as disease spreading, opinion formation, and diffusion evolve on top of these networks through the pairwise interactions of nodes [1, 4–6]. The most studied examples include simple contagion models (where "simple" refers to the fact that a contagion event can be caused by a single contact), such as the paradigmatic Susceptible-Infectious-Susceptible (SIS), widely used to describe the diffusion of a single pathogen in a population.

In reality, however, we often observe contagion processes that co-exist and affect each other [7]. Infectious diseases can indeed display complex comorbidity interactions, in which the presence of a pathogen impacts the individual susceptibility towards another pathogen [8]. For example, it is well known that HIV increases susceptibility to other sexually transmitted diseases [9]. Several research lines have extended modelling efforts in this direction to include both cooperation [10–12] and competition [13–15] between diseases. However, to date the systematic investigation of models of interacting contagion processes has been developed under two main assumptions: (*i*) they consider simple contagions, and (*ii*) they assume the interaction between processes to be symmetric, that is, bi-directional and of equal strength. Within these modeling restrictions, an interesting phenomenology has been uncovered: cooperative models can display a discontinuous transition to the epidemic state [11], and also become indistinguishable at the mean-field level from complex contagion models describing social reinforcement [16]. We recall that "complex" contagion refers to a process in which exposure to multiple sources presenting the same stimulus is needed for the contagion to occur [17].

Interactions between spreding processes are naturally not restricted to infectious diseases, as the interplay between a disease and a social behavior can also dramatically impact the resulting disease spreading dynamics [18–22]. A current and cogent example is the impact of the adoption of safe behaviors, such as the use of non-pharmaceutical interventions (hand washing, masks, self-isolation), during the COVID pandemic [22]. Motivated by this example, we challenge both restrictions described above. First, it is known that reinforcement mechanisms influence social behavior so that models of *simple* contagion—that assume independent pairwise exposures—do not offer the most adequate description [17]. *Simplicial* contagion has been proposed as an alternative approach to account for simultaneous exposures via group-contagion events [23, 24]. Such group ("higher-order") contributions were shown to induce discontinuous transitions, bi-stability and critical mass phenomena even for single processes [25–29]. Second, most contagion processes do not interact in a symmetric way. This can happen e.g. for diseases with very different time scales [30], or when considering interactions between a disease and the adoption of prudent behaviors [21], which is instead driven by a phenomenologically and analytically different social contagion process.

Here, we show that a simple contagion (describing infectious disease spreading) can exhibit the characteristics of a simplicial contagion when it is cooperatively driven by a simplicial contagion (describing the spread of a social behavior). Namely, a simple contagion in the epidemic-free regime can exhibit an abrupt transition to the epidemic regime, as well as bi-stability, if the cooperative driving by the social process is stronger than a critical value. In particular, in the asymmetrically driven case, discontinuous transitions can only take place when the driving process is simplicial, contrary to cases of bi-directional symmetric interactions. We describe the phase

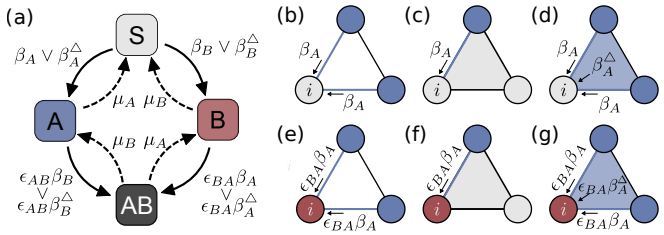

FIG. 1. The model of interacting simplicial contagions. (a) Transition probabilities between the compartments: susceptible (S, *gray*), infected exclusively by one disease (A or B, respectively *blue/red*) or by both (AB, *black*). (b)-(d) A susceptible node i can acquire A after a contact with an infectious k-simplex (this also includes AB individuals). In (d), since i is part of a 2-simplex composed by two other infectious nodes, the infection can come both from each of the two 1-faces (links) with probability β_A and from the 2-face with probability $\beta_A^{\triangle}$. (e)-(g) If i is already infected with B, the probability of getting A for each contact is affected by the coupling factor ϵ_{BA}. The same rules symmetrically apply to B instead of A. The driving process of A on B is realized by setting $\epsilon_{AB} > 1$, $\epsilon_{BA} = 1$.

diagram of the system through a mean-field (MF) approach, complemented by Markov-type simulations, and provide an analytical expression for the critical value of the cooperation. Finally, we identify effective infectivities as markers of the abrupt driven transition by rewriting the MF equations as a simple contagion with effective parameters.

The model. We consider a model for two interacting spreading processes, denoted as A and B, that also include simplicial contagions [23, 25]. Individuals are represented by a set of N nodes $\{n_i\}_{i=1}^N$ that can each be in one of four compartments, following the standard SIS framework [3]: those susceptible to both diseases (S), infected exclusively by one of the two diseases (either A or B), or by both (AB) [see Fig. 1(a)]. The compartment membership of each node i is encoded in three binary variables $x_i^\gamma \in \{0,1\}$, where $\gamma \in \{A, B, AB\}$. If node i is in state γ then $x_i^\gamma = 1$, otherwise it is zero: each node has either one non-zero or all zero variables. The density of nodes in state γ is given, at each time t, by $\rho_\gamma(t) = \frac{1}{N}\sum_{i=1}^N x_i^\gamma(t)$. The densities $\vec{\rho}(t) = \{\rho_A(t), \rho_B(t), \rho_{AB}(t)\}$ serve as macroscopic order parameters (with $\rho_S(t) = 1 - \rho_A(t) - \rho_B(t) - \rho_{AB}(t)$ the density of susceptible individuals).

Nodes can interact in pairs or larger groups, so that contagion events, which cause nodes to change compartment, take place on top of a contact structure that allows also for higher-order (non-pairwise) interactions [24, 31–33]. We mathematically represent a group encounter as a k-hyperedge, a set of $k+1$ interacting nodes [34]. For simplicity, we allow for interactions up to dimension $k = 2$. These groups involving 2 and 3 nodes are respectively called 1-hyperedges (links) and 2-hyperedges (triangles). Six parameters—three for each disease—yield contagion and recovery probabilities, as illustrated in Fig. 1. The infectivity of disease $x \in \{A, B\}$ at order $k = 1$, $\beta_{x,1} \equiv \beta_x$, is the probability per unit time for a node i susceptible to pathogen x to acquire x from an "infectious" 1-hyperedge it is part of [see Fig. 1(b)-(d)]. Similarly, $\beta_{x,2} \equiv \beta_x^{\triangle}$ control infections coming from 2-hyperedges [see Fig. 1(d)]. Note that all other nodes in the hyperedge need to be infectious for the hyperedge to be considered so. Finally, $\mu_x \in [0,1]$ denotes the standard spontaneous recovery probability (from x) per unit time.

The interaction between the two contagion processes is controlled via two additional non-negative parameters ϵ_{AB} and ϵ_{BA} that multiply the transition probabilities to a double infection (AB) from a single infection (A or B). For example, the transition $B \to AB$ occurs with probability $\epsilon_{BA}\beta_A$ from a pairwise contact with A [see Fig. 1(e)-(g)]. The two processes cooperate if $\epsilon_{xx'} > 1$ and compete if $\epsilon_{xx'} < 1$, while they are independent if $\epsilon_{xx'} = 1$. Note that the symmetry $\epsilon_{AB} = \epsilon_{BA}$ does not need to hold. Furthemore, although the model is defined on a generic higher-order structure, we focus here on simplicial complexes, a particular class of hypergraphs [24]. In a simplicial complex $\mathcal{K}$, by definition, groups of nodes are called simplices and must respect downward closure: each sub-simplex $\nu \subset \sigma$ built from subsets of a simplex $\sigma \subset \mathcal{K}$ is also part of the complex $\mathcal{K}$ [in an infectious 2-simplex thus, contagion can occur both through the 1-hyperedges contained and through the 2-hyperedge itself, see Fig. 1(d),(g)]. We make this choice for coherence with previous work [23], but it can be relaxed to more general hypergraphs [25–27, 29] without affecting the MF results.

Mean-field description. We first consider the MF description of the model, obtained under a homogeneous mixing hypothesis [35]. For simplicity, we assume identical recovery rates $\mu_A = \mu_B = \mu$ (see Sup. Mat. for the case $\mu_A \neq \mu_B$) and introduce the rescaled infectivity parameters $\lambda_x = \beta_x \langle k \rangle / \mu$ and $\lambda_x^{\triangle} = \beta_x^{\triangle} \langle k_{\triangle} \rangle / \mu$, for $x \in \{A, B\}$, where $\langle k \rangle$ and $\langle k_{\triangle} \rangle$ respectively denote the average numbers of 1- and 2-hyperedges incident on a node.

We focus on the following scenario: a simplicial contagion A that cooperatively and unidirectionally drives a simple contagion B. We thus set $\lambda_A^{\triangle} > 0$, $\lambda_B^{\triangle} = 0$, and the interactions $\epsilon_{AB} > 1$ and $\epsilon_{BA} = 1$. After rescaling time by μ and introducing the total density of nodes infected by diseases A and B, respectively $\rho_{A_{\text{tot}}} = \rho_A + \rho_{AB}$, and $\rho_{B_{\text{tot}}} = \rho_B + \rho_{AB}$ (see Sup. Mat. I), we end up with the system of coupled equations:

$$\dot{\rho}_{A_{\text{tot}}} = \rho_{A_{\text{tot}}}\left[-1 + \lambda_A(1 - \rho_{A_{\text{tot}}}) + \lambda_A^{\triangle}\rho_{A_{\text{tot}}}(1 - \rho_{A_{\text{tot}}})\right], \tag{1a}$$

$$\dot{\rho}_{B_{\text{tot}}} = \rho_{B_{\text{tot}}}\left[-1 + \lambda_B(1 - \rho_{B_{\text{tot}}}) + \lambda_B(\epsilon_{AB} - 1)(\rho_{A_{\text{tot}}} - \rho_{AB})\right], \tag{1b}$$

$$\dot{\rho}_{AB} = -2\rho_{AB} + \epsilon_{AB}\lambda_B(\rho_{A_{\text{tot}}} - \rho_{AB})\rho_{B_{\text{tot}}} + \lambda_A(\rho_{B_{\text{tot}}} - \rho_{AB})\rho_{A_{\text{tot}}} + \lambda_A^{\triangle}(\rho_{B_{\text{tot}}} - \rho_{AB})\rho_{A_{\text{tot}}}^2, \tag{1c}$$

with the additional conservation equation

$$\rho_S(t) = 1 - \rho_{A_{\text{tot}}} - \rho_{B_{\text{tot}}} + \rho_{AB}. \tag{2}$$

Note that equations (1) include two known models as specific cases. First, without interaction between the processes ($\epsilon_{AB} = \epsilon_{BA} = 1$), $\rho_{B_{\text{tot}}}$ and $\rho_{A_{\text{tot}}}$ evolve independently as a simple and simplicial contagion [23], respectively. Second, by considering

only pairwise interactions, $\lambda_A^{\triangle} = 0 = \lambda_B^{\triangle}$, A and B evolve as interacting simple contagions [8]. In general, under the conditions we set, the dynamics of $\rho_{A_{\text{tot}}}$ is decoupled from the other two variables and drives them.

We first study by numerical integration the non-equilibrium stationary state (NESS) reached by the system (1) at large times and illustrate the transitions of the corresponding value $\rho^*_{B_{\text{tot}}} = \lim_{t\to\infty} \rho_{B_{\text{tot}}}(t)$ in Fig. 2. The most interesting case is given by $\lambda_B < 1$, for which —without a driving process A— the simple contagion process B would be in the epidemic-free absorbing state ($\rho^*_{B_{\text{tot}}} = 0$). We thus illustrate how the B epidemic NESS $\rho^*_{B_{\text{tot}}}$ depends on the parameters of the driver A, on the coupling ϵ_{AB}, and how it can transition to the epidemic active state, despite having $\lambda_B < 1$. If $\lambda_A^{\triangle} \leq 1$, we always obtain a continuous transition for $\rho^*_{B_{\text{tot}}}$ [see Fig. 2(a,b)]. On the other hand, if $\lambda_A^{\triangle} > 1$, the driven process can exhibit a discontinuous transition [see Fig. 2(c,d)]. More precisely, the transition changes from continuous to discontinuous when the coupling parameter ϵ_{AB} becomes larger than a critical value ϵ^c_{AB}. Above this threshold ($\epsilon_{AB} > \epsilon^c_{AB}$, black circles in Fig. 2c), there is a discontinuous transition at a critical value λ^c_A that does not depend on ϵ_{AB}. For weaker cooperation ($\epsilon_{AB} < \epsilon^c_{AB}$, white and grey symbols in Fig. 2c), a continuous transition occurs from $\rho^*_{B_{\text{tot}}} = 0$ to the epidemic state $\rho^*_{B_{\text{tot}}} > 0$ when λ_A crosses another critical value $\lambda'^c_A \geq \lambda^c_A$ that decreases as ϵ_{AB} increases (and $\lambda'^c_A \to \lambda^c_A$ in the limit $\epsilon_{AB} \to \epsilon^c_{AB}$). Moreover, the epidemic-free absorbing state $\rho^*_{B_{\text{tot}}} = 0$ remains stable as long as $\lambda_A < 1$, so that there is a region of bi-stability $\lambda^c_A < \lambda_A < 1$ (shaded region) for $\epsilon_{AB} > \epsilon^c_{AB}$, and bi-stability can also be observed when $\epsilon_{AB} < \epsilon^c_{AB}$ in the region $\lambda'^c_A < \lambda_A < 1$ (grey symbols). Hence, the simple contagion B exhibits characteristics of simplicial contagion— an abrupt transition and bi-stability—due to the driving of the simplicial contagion A.

To analytically explain this behavior, we need to find the NESS by setting $\dot{\rho}_x = 0$. We can first directly solve $\dot{\rho}_{A_{\text{tot}}} = 0$, as Eq. (1a) exactly maps back to the single simplicial contagion analysed in Ref. [23]. It presents a trivial solution $\rho^*_{A_{\text{tot}}} = 0$ and two other NESS $\rho^{*,\pm}_{A_{\text{tot}}}$ (see Sup. Mat. II), which are physically valid only when non-negative. We also know that $\lambda_A^{\triangle}$ controls the type of transition to the epidemic state [23]. That is, for $\lambda_A^{\triangle} \leq 1$, the bifurcation diagram has a continuous transition at $\lambda_A = 1$ from $\rho^*_{A_{\text{tot}}} = 0$ to the epidemic state $\rho^{*,+}_{A_{\text{tot}}}$. When instead $\lambda_A^{\triangle} > 1$, a discontinuous transition to $\rho^{*,+}_{A_{\text{tot}}}$ occurs at $\lambda^c_A = -\lambda_A^{\triangle} + 2\sqrt{\lambda_A^{\triangle}} \leq 1$. The epidemic-free state remains stable for $\lambda_A \leq 1$, but becomes unstable above: This leads to bi-stability in the parameter region $\{\lambda_A^{\triangle} > 1, \lambda^c_A \leq \lambda_A \leq 1\}$. The discontinuous transition is therefore the direct consequence of a sufficiently strong three-body (higher-order) interaction in A ($\lambda_A^{\triangle} > 1$).

We now need to solve the two-dimensional system $(\rho_{B_{\text{tot}}}, \rho_{AB})$. It is decoupled in the absorbing state $(0, 0)$ only, which is always stable for ρ_{AB}, but stable for $\rho_{B_{\text{tot}}}$ only if $\lambda_B < 1$. While the non-trivial analytical solutions can be found explicitly, the corresponding formula are rather complicated and do not easily provide insights; we thus leave them to Sup. Mat. II. Instead, we discuss here the implicit solutions for $\rho^*_{B_{\text{tot}}}$, given by

$$\rho^{*,\pm}_{B_{\text{tot}}} = 1 - \frac{1}{\lambda_B} + (\rho^{*,\pm}_{A_{\text{tot}}} - \rho^{*,\pm}_{AB})(\epsilon_{AB} - 1). \qquad (3)$$

Equation (3) implicitly contains two solutions $\pm$ from $\rho^{*,\pm}_{A_{\text{tot}}}$ and $\rho^{*,\pm}_{AB}$.

We can now explain the behavior shown in Fig. 2. If $\lambda_A^{\triangle} < 1$ [Figs. 2(a,b)], $\rho^*_{A_{\text{tot}}}$ exhibits a continuous transition at $\lambda_A = 1$, below which it is zero. This implies that ρ_{AB} also goes to the absorbing state if $\lambda_A < 1$. Hence, from Eq. (3), we have $\lim_{\lambda_A \to 1^+} \rho^{*,\pm}_{B_{\text{tot}}} \leq 0$ (remember $\lambda_B < 1$) and, as λ_A increases above 1, $\rho^{*,+}_{A_{\text{tot}}}$ increases continuously [23], leading $\rho^{*,\pm}_{B_{\text{tot}}}$ to also cross continuously 0 at a certain $\lambda_A \geq 1$. For $\lambda_A^{\triangle} \geq 1$ instead, $\rho^*_{A_{\text{tot}}}$ has a discontinuous transition at $\lambda_A = \lambda^c_A$ which implies that ρ^*_{AB} has one too. Consequently, from Eq. (3), since $\lambda_B < 1$, we have $\lim_{\lambda_A \to \lambda^{c,-}_A} \rho^*_{B_{\text{tot}}} = 0$, but $\lim_{\lambda_A \to \lambda^{c,+}_A} \rho^{*,\pm}_{B_{\text{tot}}} > 0$ above a certain value $\epsilon_{AB} > \epsilon^c_{AB}$. Hence, this critical value ϵ^c_{AB} can be derived analytically by solving $\rho^{*,+}_{B_{\text{tot}}} = 0$ at λ^c_A. In other words, we find the critical driving strength ϵ^c_{AB} by finding the $\rho^{*,+}_{B_{\text{tot}}}$ curve, between the grey and black curves in Fig. 2(c), such that it reaches zero at λ^c_A. This corresponds to the case $\lambda_B \leq 1$, $\lambda_A^{\triangle} > 1$ which we denoted region I. Similarly, if $\lambda_B > 1$ instead (with $\lambda_A^{\triangle} > 1$, region II), it suffices solving $\rho^{*,+}_{B_{\text{tot}}} = 1 - 1/\lambda_B$ at λ^c_A because $1 - 1/\lambda_B$ is

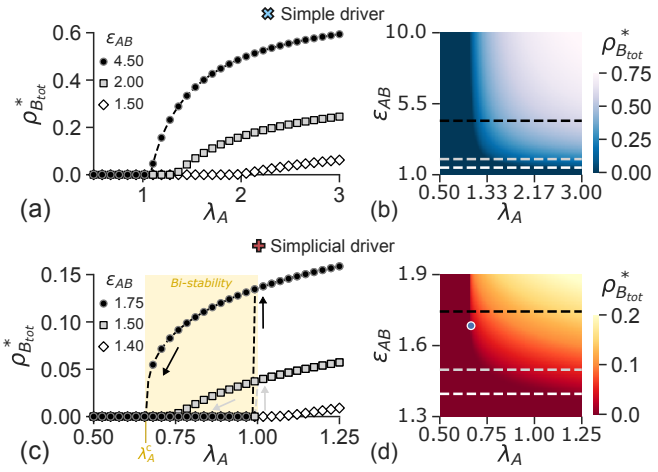

FIG. 2. A simplicial driver can induce a discontinuous transition (c,d), contrary to a simple driver (a,b). We show the stable NESS of $\rho^*_{B_{\text{tot}}}$ in the MF Eqs. (1), as the driving process for A follows a simple contagion (a,b), with $\lambda_A^{\triangle} = 0$, or a simplicial contagion (c,d), with $\lambda_A^{\triangle} = 2.5$ [$\lambda_B = 0.8$, $\lambda_B^{\triangle} = 0$]. Note the different scales on the x-axes. (a,c) The stationary solutions for $\rho^*_{B_{\text{tot}}}$ are plotted as a function of the rescaled pairwise infectivity λ_A for three values of the driving strength ϵ_{AB}. In (c), the transition of the simple contagion B becomes discontinuous above a critical value of cooperation ϵ^c_{AB}. (b,d) Heatmaps of $\rho^*_{B_{\text{tot}}}$ as a function of λ_A and ϵ_{AB}. Dashed horizontal lines correspond to the selected ϵ_{AB} values shown in (a) and (b) respectively. The blue dot in (d) highlights the critical point $(\lambda^c_A, \epsilon^c_{AB})$. The blue and red crosses represent a visual hint to locate the results within the full phase diagram of Fig. 3.

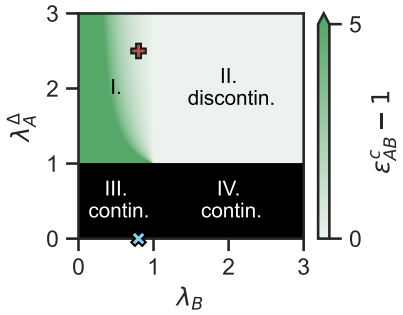

FIG. 3. The phase diagram in the $(\lambda_B, \lambda_A^\triangle)$ parameter space has four regions. In region I ($\lambda_B \leq 1$, $\lambda_A^\triangle > 1$), $\rho^*_{B_{\text{tot}}}$ undergoes an abrupt transition if the driving cooperation is strong enough, $\epsilon_{AB} > \epsilon^c_{AB}$. The value of ϵ^c_{AB} is represented by shades of green. For visual clarity, the green scale is truncated at a maximum value of 5, so that larger values are represented by the same color as 5. The red cross corresponds to the case shown in Figs. 2(c,d). In region II ($\lambda_B > 1$, $\lambda_A^\triangle > 1$), $\epsilon^c_{AB} = 1$ and the transition is discontinuous for all ϵ_{AB}. For $\lambda_A^\triangle \leq 1$, that is regions III and IV, the transition is always continuous. The blue cross indicates the case shown in Figs. 2(a,b).

now the pre-transition NESS. Finally, the solution is given by

$$\epsilon^c_{AB} = \begin{cases} \frac{\sqrt{\lambda_A^\triangle} - \lambda_B}{\left(\sqrt{\lambda_A^\triangle} - 1\right)\lambda_B} & \text{in region I,} \\ 1 & \text{in region II,} \end{cases} \tag{4}$$

which is shown in Fig. 3. In region I, increasing $\lambda_A^\triangle$ or λ_B make ϵ^c_{AB} decrease, so that discontinuous transitions are obtained for smaller values of driving strength ϵ_{AB}. In fact, $\epsilon^c_{AB} \to +\infty$ as $\lambda_A^\triangle \to 1$ or $\lambda_B \to 0$. In region II, $\epsilon^c_{AB} = 1$ so that all values of cooperation $\epsilon_{AB} > 1$ yield a discontinuous transition. Finally, no critical value of cooperation can be defined in regions III and IV, where transitions are always continuous.

Effective formalism. For $\epsilon_{AB} > \epsilon^c_{AB}$ —that is, when simplicial behavior is possible for B— the driven process B will exhibit discontinuous transitions and bi-stability as a function of λ_A. To illustrate how this phenomenology emerges, we can rewrite the dynamics of B as an effective simple contagion. We follow ideas from Ref. [16] to rewrite the MF equation of the single simplicial $\rho_{A_{\text{tot}}}$ from Eq. (1a) as a simple contagion with effective infectivity $\tilde{\lambda}_A = \lambda_A + \lambda_A^\triangle \rho_{A_{\text{tot}}}$. We then rewrite Eq. (1b) of the driven $\rho_{B_{\text{tot}}}$ as a simple contagion

$$\dot{\rho}_{B_{\text{tot}}} = -\rho_{B_{\text{tot}}} + \tilde{\lambda}_B \, \rho_{B_{\text{tot}}}[1 - \rho_{B_{\text{tot}}}], \tag{5}$$

with effective infectivity

$$\tilde{\lambda}_B = \lambda_B + \lambda_B(\epsilon_{AB} - 1)\frac{1}{1 - \rho_{B_{\text{tot}}}}\rho_A. \tag{6}$$

This expression can be cast into the same form as $\tilde{\lambda}_A$ by defining an effective simplicial infectivity

$$\tilde{\lambda}_B^\triangle = \lambda_B(\epsilon_{AB} - 1)\frac{\rho_A}{\rho_{B_{\text{tot}}}(1 - \rho_{B_{\text{tot}}})}, \tag{7}$$

which implicitly depends on λ_A and $\lambda_A^\triangle$ through ρ_A (see Fig. 4). If there is no interaction ($\epsilon_{AB} = 1$), we recover

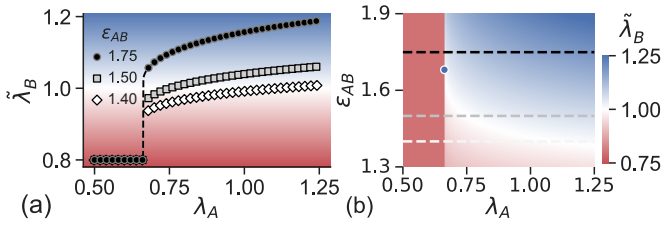

FIG. 4. The discontinuous nature of the driven contagion B can be determined from its effective infectivity $\tilde{\lambda}_B$. We show $\tilde{\lambda}_B$ for a range of cooperation ϵ_{AB} and infectivity λ_A values, corresponding to the curves in Fig. 2(c). The dot in panel (b) shows the critical point $(\lambda^c_A, \epsilon^c_{AB})$.

$\tilde{\lambda}_B = \lambda_B$ and the effective simplicial infectivity vanishes, $\tilde{\lambda}_B^\triangle = 0$, as expected. More importantly, the effective $\tilde{\lambda}_B$ has a critical value of 1 which can help distinguish between the transitions observed in Fig. 2. Indeed, $\tilde{\lambda}_B$ is the effective infectivity parameter of the simple contagion that has stationary solutions given by $1 - 1/\tilde{\lambda}_B$. We know this solution has a critical value $\tilde{\lambda}_B = 1$ below which the only stable solution is 0, and above which it is positive. Thus, the driven contagion B has a transition to an epidemic state if and only if $\tilde{\lambda}_B$ crosses 1 as λ_A increases. Moreover, that transition is discontinuous if and only if the transition of $\tilde{\lambda}_B$ across one is discontinuous. This can be seen by comparing the three curves in Fig. 4(a) to the corresponding curves for $\rho^*_{B_{\text{tot}}}$ in Fig. 2(c).

Temporal properties. The bifurcation diagrams in Figs. 2, 3, and 4 give us a clear picture of the asymptotic states, but lack information about the temporal evolution of trajectories, which, in practical settings, are often the only data available. Let us consider a case where we would only be able to observe the spreading of disease B via $\rho_{B_{\text{tot}}}(t)$, while the driving social contagion process A is unobservable. Interestingly, the evolution of the observed simple contagion B depends then on the initial conditions of the hidden process A. To show this, and further confirm the phenomenology described beyond the homogeneous mixing hypothesis adopted in the MF approach, we shift to a Markov-chain formalism [36, 37]—able to encode a non-trivial interaction structure between nodes (see Sup. Mat. III for the corresponding set of equations). We consider a synthetic random simplicial complex, constructed with the generative model introduced in Ref. [23], with $N = 2000$ nodes and generalized average degrees $\langle k \rangle = 20$ and $\langle k^\triangle \rangle = 6$ [24], and integrate the Markov equations to follow the temporal evolution of the system.

We place ourselves in the same scenario of the black curve ($\epsilon_{AB} = 1.75$) of Fig. 2(b), that is, with a simplicial driver A ($\lambda_A^\triangle = 2.5$). We fix all other parameters, including the initial condition $\rho_{B_{\text{tot}}}(0)$, but vary the initial condition of the driver, $\rho_{A_{\text{tot}}}(0)$. Results are shown in Fig. 5. If the driver contagion A is in the endemic regime (but not in the bi-stability region, e.g. $\lambda_A = 1.2$), $\rho_{B_{\text{tot}}}$ reaches the same NESS for all values of $\rho_{A_{\text{tot}}}(0)$, but with different transient dynamics. This affects the relaxation time, and the evolution can even be non-monotonic [Fig. 5(a)]. Moreover, if the simplicial driver is in the bi-stability region ($\lambda_A = 0.7$), it induces bi-stability

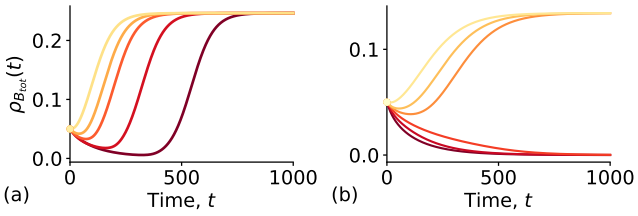

FIG. 5. The temporal evolution of the simple contagion B is affected by the initial conditions of the (hidden) simplicial driver A. We show $\rho_{B_{\text{tot}}}$ over time, for A in (a) the endemic region, $\lambda_A = 1.2$, and (b) the bi-stable region, $\lambda_A = 0.7$. Shades of red represent a range of initial conditions of the driver $\rho_A(0) \in [0.001, 0.35]$. In (b), the—simple contagion—process B can reach one of two stationary states, depending on those initial conditions. Other parameters are set to $\lambda_B = 0.8$, $\lambda_B^{\triangle} = 0$, $\epsilon_{AB} = 1.75$, and $\lambda_A^{\triangle} = 2.5$.

in the—otherwise simple—process B. Specifically, $\rho_{B_{\text{tot}}}(t)$ can reach two different states, depending on the driving initial condition, even though all "visible" B parameters are fixed [Fig. 5(a)]. Note that this bi-stability emerges only if the driving is simplicial with $\lambda_A^{\triangle} > 1$ (see also Sup. Mat. Fig. S1).

In conclusion, we have introduced a model of interacting simplicial contagions, focusing on the case where a simple contagion—that can represent the spread of a disease—is cooperatively driven by a (potentially hidden) simplicial one describing behavioral spread. We showed numerically and analytically that the simple contagion can then exhibit an abrupt transition to the epidemic state and bi-stability, but only if the driving process behaves as a "truly" simplicial one, i.e., $\lambda_A^{\triangle} \geq 1$. The results highlight that an abrupt transition in the observed process can occur as a function of the control parameter of a second—potentially hidden—driver process. Consider the situation of an observer of an epidemic process, who does not know whether it is simple or driven by some underlying reinforcing mechanisms of complex contagion, leading to discontinuous behaviors. A natural intervention would then be to try to reduce the intrinsic infectivity of the spreading pathogen, for example through pharmaceutical interventions or reduction of social contacts (e.g. sanitary lockdowns): this would however lead only to a continuous change in the incidence. However, if the spread is driven by an underlying complex contagion, acting on the hidden driver process (e.g. promoting social adoption of safe behaviors) could result in a more effective strategy and lead to an abrupt transition to the epidemic-free state (if the interaction is strong enough $\epsilon_{AB} > \epsilon_{AB}^c$). Finally, different populations could be characterised by different properties of the hidden behavioral contagion process (heterogeneous λ_A and $\lambda_A^{\triangle}$ values), thus leading to a large diversity of temporal evolutions, and—potentially—of final outcomes of the pathogen's spread, without the need for different intrinsic infectivity properties of the pathogen across these populations.

Results also suggest that other driving spreading processes could yield a similar phenomenology if they exhibit a discontinuous transition, inducing a change from a continuous to a discontinuous transition in the driven process. We note in this context that the framework of Ref. [38] suggests a universal route to abrupt transitions, achieved through the addition of a control parameter to a process that displays a continuous phase transition. However, the situation that we have explored here broadens the picture. Indeed, if both spreading processes are simple contagions, it appears that a bi-directional interaction (leading to a feedback loop) is an additional necessary condition for a discontinuous transition to emerge. In the case of a unidirectional coupling, instead, the driving process needs to be itself simplicial with bi-stability. It seems thus that this provides a novel, different route to the emergence of abrupt transitions. The exact conditions under which these routes apply to coupled systems would be an interesting direction for future works. Another interesting perspective consists in the analysis of real-world data and the development of tools to detect the simple, complex or coupled character of a process from observed time series [39] (as well potentially as the full reconstruction of the interactions [40]).

I.I. acknowledges support from the James S. McDonnell Foundation 21st Century Science Initiative Understanding Dynamic and Multi-scale Systems - Postdoctoral Fellowship Award. A.B. acknowledges support from the Agence Nationale de la Recherche (ANR) project DATAREDUX (ANR-19-CE46-0008). M.L. and G.P. acknowledge partial support from Intesa Sanpaolo Innovation Center during the preparation of this work.

* I.I. and M.L. contributed equally to this work.
† A.B and G.P. jointly supervised this work.

[1] A. Barrat, M. Barthélemy, and A. Vespignani, *Dynamical Processes on Complex Networks* (Cambridge University Press, 2008).
[2] A. Vespignani, Modelling dynamical processes in complex socio-technical systems, Nat. Phys. **8**, 32 (2012).
[3] R. Pastor-Satorras, C. Castellano, P. Van Mieghem, and A. Vespignani, Epidemic processes in complex networks, Rev. Mod. Phys. **87**, 925 (2015).
[4] D. J. Daley and D. G. Kendall, Epidemics and rumours, Nature **204**, 1118 (1964).
[5] R. Pastor-Satorras and A. Vespignani, Epidemic spreading in scale-free networks, Phys. Rev. Lett. **86**, 3200 (2001).
[6] E. Rogers, *Diffusion of Innovations, 5th Edition* (Free Press, 2003).
[7] J. Sanz, C.-Y. Xia, S. Meloni, and Y. Moreno, Dynamics of interacting diseases, Phys. Rev. X **4**, 041005 (2014).
[8] W. Wang, Q.-H. Liu, J. Liang, Y. Hu, and T. Zhou, Coevolution spreading in complex networks, Phys. Rep. **820**, 1 (2019).
[9] J.-A. Røttingen, D. W. Cameron, and G. P. Garnett, A systematic review of the epidemiologie interactions between classic sexually transmitted diseases and hiv: How much really is known?, Sex. Transm. Dis. , 579 (2001).
[10] W. Cai, L. Chen, F. Ghanbarnejad, and P. Grassberger, Avalanche outbreaks emerging in cooperative contagions, Nat. Phys. **11**, 936 (2015).
[11] L. Chen, F. Ghanbarnejad, and D. Brockmann, Fundamental properties of cooperative contagion processes, New J. Phys. **19**, 103041 (2017).

[12] P.-B. Cui, F. Colaiori, C. Castellano, *et al.*, Mutually cooperative epidemics on power-law networks, Phys. Rev. E **96**, 022301 (2017).

[13] B. Karrer and M. E. Newman, Competing epidemics on complex networks, Phys. Rev. E **84**, 036106 (2011).

[14] C. Poletto, S. Meloni, A. Van Metre, V. Colizza, Y. Moreno, and A. Vespignani, Characterising two-pathogen competition in spatially structured environments, Sci. Rep. **5**, 1 (2015).

[15] W. Li, X. Xue, L. Pan, T. Lin, and W. Wang, Competing spreading dynamics in simplicial complex, Appl. Math. Comput. **412**, 126595 (2022).

[16] L. Hébert-Dufresne, S. V. Scarpino, and J.-G. Young, Macroscopic patterns of interacting contagions are indistinguishable from social reinforcement, Nat. Phys. **16**, 426 (2020).

[17] D. Centola and M. Macy, Complex contagions and the weakness of long ties, Am. J. Sociol. **113**, 702 (2007).

[18] S. Funk, M. Salathé, and V. Jansen, Modelling the inuence of human behaviour on the spread of infectious diseases: a review, J. R. Soc. Interface **7**, 1247 (2010).

[19] N. Perra, D. Balcan, B. Gonçalves, and A. Vespignani, Towards a characterization of behavior-disease models, PLoS One **6**, e23084 (2011).

[20] C. Granell, S. Gómez, and A. Arenas, Dynamical interplay between awareness and epidemic spreading in multiplex networks, Phys. Rev. Lett. **111**, 128701 (2013).

[21] S. V. Scarpino, A. Allard, and L. Hébert-Dufresne, The effect of a prudent adaptive behaviour on disease transmission, Nat. Phys. **12**, 1042 (2016).

[22] N. Perra, Non-pharmaceutical interventions during the covid-19 pandemic: A review, Phys. Rep. **913**, 1 (2021).

[23] I. Iacopini, G. Petri, A. Barrat, and V. Latora, Simplicial models of social contagion, Nat. Commun. **10**, 1 (2019).

[24] F. Battiston, G. Cencetti, I. Iacopini, V. Latora, M. Lucas, A. Patania, J.-G. Young, and G. Petri, Networks beyond pairwise interactions: Structure and dynamics, Phys. Rep. **874**, 1 (2020).

[25] A. Barrat, G. Ferraz de Arruda, I. Iacopini, and Y. Moreno, Social contagion on higher-order structures, in *Higher-Order Systems* (Springer, 2022) pp. 329–346.

[26] N. W. Landry and J. G. Restrepo, The effect of heterogeneity on hypergraph contagion models, Chaos **30**, 103117 (2020).

[27] G. Ferraz de Arruda, M. Tizzani, and Y. Moreno, Phase transitions and stability of dynamical processes on hypergraphs, Commun. Phys. **4**, 24 (2021).

[28] J. T. Matamalas, S. Gómez, and A. Arenas, Abrupt phase transition of epidemic spreading in simplicial complexes, Phys. Rev. Research **2**, 012049 (2020).

[29] G. St-Onge, I. Iacopini, V. Latora, A. Barrat, G. Petri, A. Allard, and L. Hébert-Dufresne, Influential groups for seeding and sustaining nonlinear contagion in heterogeneous hypergraphs, Commun. Phys. **5**, 1 (2022).

[30] P. C. Ventura, Y. Moreno, and F. A. Rodrigues, Role of time scale in the spreading of asymmetrically interacting diseases, Phys. Rev. Research **3**, 013146 (2021).

[31] R. Lambiotte, M. Rosvall, and I. Scholtes, From networks to optimal higher-order models of complex systems, Nat. Phys. 10.1038/s41567-019-0459-y (2019).

[32] C. Bick, E. Gross, H. A. Harrington, and M. T. Schaub, What are higher-order networks?, arXiv preprint arXiv:2104.11329 https://doi.org/10.48550/arXiv.2104.11329 (2021).

[33] F. Battiston, E. Amico, A. Barrat, G. Bianconi, G. Ferraz de Arruda, B. Franceschiello, I. Iacopini, S. Kéfi, V. Latora, Y. Moreno, M. Murray, T. Peixoto, F. Vaccarino, and G. Petri, The physics of higher-order interactions in complex systems, Nat. Phys. **17**, 1093 (2021).

[34] L. Torres, A. S. Blevins, D. Bassett, and T. Eliassi-Rad, The why, how, and when of representations for complex systems, SIAM Rev. **63**, 435 (2021).

[35] I. Kiss, J. Miller, and P. Simon, *Mathematics of Epidemics on Networks: From Exact to Approximate Models*, Interdisciplinary Applied Mathematics (Springer International Publishing, 2017).

[36] S. Gómez, A. Arenas, J. Borge-Holthoefer, S. Meloni, and Y. Moreno, Discrete-time markov chain approach to contact-based disease spreading in complex networks, Europhys. Lett. **89**, 38009 (2010).

[37] D. Soriano-Paños, F. Ghanbarnejad, S. Meloni, and J. Gómez-Gardeñes, Markovian approach to tackle the interaction of simultaneous diseases, Phys. Rev. E **100**, 062308 (2019).

[38] C. Kuehn and C. Bick, A universal route to explosive phenomena, Sci. Adv. **7**, eabe3824 (2021).

[39] T. Brett, M. Ajelli, Q.-H. Liu, M. G. Krauland, J. J. Grefenstette, W. G. van Panhuis, A. Vespignani, J. M. Drake, and P. Rohani, Detecting critical slowing down in high-dimensional epidemiological systems, PLoS Comput. Biol. **16**, e1007679 (2020).

[40] T. P. Peixoto, Network reconstruction and community detection from dynamics, Phys. Rev. Lett. **123**, 128301 (2019).

Supplementary Material: Simplicially driven simple contagion

I. MEAN-FIELD DESCRIPTION

The general mean field equations describing the evolution of the densities are:

$$\dot{\rho}_A = -\rho_A + \lambda_A\rho_S(\rho_A+\rho_{AB}) + \lambda_A^{\triangle}\rho_S(\rho_A+\rho_{AB})^2 + \rho_{AB} - \epsilon_{AB}\lambda_B\rho_A(\rho_B+\rho_{AB}) - \epsilon_{AB}\lambda_B^{\triangle}\rho_A(\rho_B+\rho_{AB})^2 \tag{S1a}$$

$$\dot{\rho}_B = -\rho_B + \lambda_B\rho_S(\rho_B+\rho_{AB}) + \lambda_B^{\triangle}\rho_S(\rho_B+\rho_{AB})^2 + \rho_{AB} - \epsilon_{BA}\lambda_A\rho_B(\rho_A+\rho_{AB}) - \epsilon_{BA}\lambda_A^{\triangle}\rho_B(\rho_A+\rho_{AB})^2 \tag{S1b}$$

$$\dot{\rho}_{AB} = -2\rho_{AB} + \epsilon_{AB}\lambda_B\rho_A(\rho_B+\rho_{AB}) + \epsilon_{AB}\lambda_B^{\triangle}\rho_A(\rho_B+\rho_{AB})^2 + \epsilon_{BA}\lambda_A\rho_B(\rho_A+\rho_{AB}) + \epsilon_{BA}\lambda_A^{\triangle}\rho_B(\rho_A+\rho_{AB})^2 \tag{S1c}$$

with the additional condition that

$$\rho_S = 1 - \rho_A - \rho_B - \rho_{AB}. \tag{S2}$$

As explained in the main text, we focus on the case $\epsilon_{BA} = 1$, $\lambda_B^{\triangle} = 0$, so that Eq. (S1) becomes

$$\dot{\rho}_A = -\rho_A + \lambda_A\rho_S(\rho_A+\rho_{AB}) + \lambda_A^{\triangle}\rho_S(\rho_A+\rho_{AB})^2 + \rho_{AB} - \epsilon_{AB}\lambda_B\rho_A(\rho_B+\rho_{AB}) \tag{S3a}$$

$$\dot{\rho}_B = -\rho_B + \lambda_B\rho_S(\rho_B+\rho_{AB}) + \rho_{AB} - \lambda_A\rho_B(\rho_A+\rho_{AB}) - \lambda_A^{\triangle}\rho_B(\rho_A+\rho_{AB})^2 \tag{S3b}$$

$$\dot{\rho}_{AB} = -2\rho_{AB} + \epsilon_{AB}\lambda_B\rho_A(\rho_B+\rho_{AB}) + \lambda_A\rho_B(\rho_A+\rho_{AB}) + \lambda_A^{\triangle}\rho_B(\rho_A+\rho_{AB})^2 \tag{S3c}$$

Then, we apply the following change of variables: $\rho_{A_{\text{tot}}} = \rho_A + \rho_{AB}$, $\rho_{B_{\text{tot}}} = \rho_B + \rho_{AB}$. This yields

$$\dot{\rho}_{A_{\text{tot}}} = (-\rho_A - \rho_{AB}) + \lambda_A\rho_{A_{\text{tot}}}[1 - \rho_{B_{\text{tot}}} - \rho_A + \rho_B] + \lambda_A^{\triangle}\rho_{A_{\text{tot}}}^2[1 - \rho_{B_{\text{tot}}} - \rho_A + \rho_B] \tag{S4a}$$

$$\dot{\rho}_{B_{\text{tot}}} = (-\rho_B - \rho_{AB}) + \lambda_B\rho_{B_{\text{tot}}}[1 - \rho_{A_{\text{tot}}} - \rho_B + \epsilon_{AB}\rho_A] \tag{S4b}$$

$$\dot{\rho}_{AB} = -2\rho_{AB} + \epsilon_{AB}\lambda_B\rho_A\rho_{B_{\text{tot}}} + \lambda_A\rho_B\rho_{A_{\text{tot}}} + \lambda_A^{\triangle}\rho_B\rho_{A_{\text{tot}}}^2 \tag{S4c}$$

We further rewrite this by replacing all remaining ρ_A and ρ_B, and using the identity $1 - \rho_{B_{\text{tot}}} - \rho_A + \rho_B = 1 - \rho_{A_{\text{tot}}}$,

$$\dot{\rho}_{A_{\text{tot}}} = -\rho_{A_{\text{tot}}} + \lambda_A\rho_{A_{\text{tot}}}[1 - \rho_{A_{\text{tot}}}] + \lambda_A^{\triangle}\rho_{A_{\text{tot}}}^2[1 - \rho_{A_{\text{tot}}}] \tag{S5a}$$

$$\dot{\rho}_{B_{\text{tot}}} = -\rho_{B_{\text{tot}}} + \lambda_B\rho_{B_{\text{tot}}}[1 - \rho_{A_{\text{tot}}} - \rho_{B_{\text{tot}}} + \rho_{AB} + \epsilon_{AB}(\rho_{A_{\text{tot}}} - \rho_{AB})] \tag{S5b}$$

$$\dot{\rho}_{AB} = -2\rho_{AB} + \epsilon_{AB}\lambda_B(\rho_{A_{\text{tot}}} - \rho_{AB})\rho_{B_{\text{tot}}} + \lambda_A(\rho_{B_{\text{tot}}} - \rho_{AB})\rho_{A_{\text{tot}}} + \lambda_A^{\triangle}(\rho_{B_{\text{tot}}} - \rho_{AB})\rho_{A_{\text{tot}}}^2 \tag{S5c}$$

which can be refactored to obtain Eqs. (1) from the main text.

II. DERIVATION OF THE MEAN-FIELD FIXED POINTS

Equation (1a) in the main text is the same as the simplicial contagion from Ref. [23]. Its non-trivial solutions are

$$\rho_{A_{\text{tot}}}^{*,\pm} = \frac{(\lambda_A^{\triangle} - \lambda_A) \pm \sqrt{(\lambda_A - \lambda_A^{\triangle})^2 + 4\lambda_A^{\triangle}(\lambda_A - 1)}}{2\lambda_A^{\triangle}}. \tag{S6}$$

The remaining two-dimensional system $(\rho_{B_{\text{tot}}}, \rho_{AB})$ can be solved analytically by hand or with the help of software like *Mathematica*. The implicit solution for Eq. (1a) in the main text is given by Eq. (3).

To solve for ρ_{AB}, we rewrite Eq. (1c) from the main text by factorising and setting the left-hand-side to zero:

$$0 = -2\rho_{AB} + \epsilon_{AB}\lambda_B(\rho_{A_{\text{tot}}} - \rho_{AB})\rho_{B_{\text{tot}}} + \lambda_A(\rho_{B_{\text{tot}}} - \rho_{AB})\rho_{A_{\text{tot}}} + \lambda_A^{\triangle}(\rho_{B_{\text{tot}}} - \rho_{AB})\rho_{A_{\text{tot}}}^2, \tag{S7}$$

$$= \rho_{AB}\left[-2 - \epsilon_{AB}\lambda_B\rho_{B_{\text{tot}}} - \lambda_A\rho_{A_{\text{tot}}} - \lambda_A^{\triangle}\rho_{A_{\text{tot}}}^2\right] + \rho_{A_{\text{tot}}}\rho_{B_{\text{tot}}}\left[\epsilon_{AB}\lambda_B + \lambda_A + \lambda_A^{\triangle}\rho_{A_{\text{tot}}}\right], \tag{S8}$$

from which we already see that $\rho_{AB}^* = 0$ if $\rho_{A_{\text{tot}}} = 0$ or $\rho_{B_{\text{tot}}} = 0$. Now, we inject the expression of $\rho_{B_{\text{tot}}}$ from Eq. (3) and cast the equation into the usual quadratic form in ρ_{AB}:

$$0 = A\rho_{AB}^2 + B\rho_{AB} + C, \tag{S9}$$

where

$$A = +\epsilon_{AB}\lambda_B E^-_{AB}, \tag{S10}$$
$$B = -2-\epsilon_{AB}\lambda_B(\Lambda^-_B + E^-_{AB}\rho^*_{A_{\text{tot}}}) - (\lambda_A + E^-_{AB}K)\rho^*_{A_{\text{tot}}} - \lambda^{\triangle}_A \rho^{*2}_{A_{\text{tot}}}, \tag{S11}$$
$$C = \rho^*_{A_{\text{tot}}} K(\Lambda^-_B + E^-_{AB}\rho^*_{A_{\text{tot}}}). \tag{S12}$$

To shorten the notation, we have also defined

$$E^-_{AB} = \epsilon_{AB} - 1, \tag{S13}$$
$$\Lambda^-_i = 1 - 1/\lambda_i, \tag{S14}$$
$$K = \epsilon_{AB}\lambda_B + \lambda_A + \lambda^{\triangle}_A \rho^*_{A_{\text{tot}}}. \tag{S15}$$

The non-zero solutions for ρ_{AB} the usual quadratic solution

$$\rho^{*,\pm}_{AB} = \frac{-B \pm \sqrt{B^2 - 4AC}}{2A}, \tag{S16}$$

which, unfolded, is an expression in terms of the parameters of the system only. These together with $\rho^*_{A_{\text{tot}}}$ can be re-injected into Eq. (3) for $\rho^*_{B_{\text{tot}}}$ to close the system.

III. MARKOV-CHAIN APPROACH

Here we write a system of coupled Markov-chain equations which govern the microscopic evolution of our model [36, 37]. More precisely, we can write down the conditional probability $P(x^\gamma_i(t+1) = 1|\mathbf{x}(t), \theta, \mathbf{A}) \equiv p^i_\gamma(t)$ of finding each node i in state $\gamma = \{S, A, B, AB\}$ at time $t+1$ given the probability vector representing the status of all nodes at time t $\mathbf{x}(t) = x^\gamma_i(t)$, the model parameters $\theta = \{\beta_A, \beta^{\triangle}_A, \beta_B, \beta^{\triangle}_B, \mu_A, \mu_B, \epsilon_{AB}, \epsilon_{BA}\}$, and the structure $\mathbf{A}$. Using the simplified notation $p^i_\gamma(t)$, we impose that, at each time,

$$p^i_S(t) = 1 - p^i_A(t) - p^i_B(t) - p^i_{AB}(t). \tag{S17}$$

The Markov-chain equations for the three states are the following:

$$p^i_{AB}(t+1) = p^i_b(t)(1-\mu_B)(1-q^i_A(t)) + p^i_A(t)(1-\mu_A)(1-q^i_B(t)) + p^i_{AB}(t)(1-\mu_A)(1-\mu_B) \tag{S18a}$$
$$p^i_A(t+1) = p^i_{AB}(t)\mu_B(1-\mu_A) + p^i_A(t)(1-\mu_A)q^i_B(t) + p^i_B(t)\mu_B(1-q^i_A(t)) + p^i_S(t)(1-q^i_{AB}(t))f^i_A(t) \tag{S18b}$$
$$p^i_B(t+1) = p^i_{AB}(t)\mu_A(1-\mu_B) + p^i_B(t)(1-\mu_B)q^i_A(t) + p^i_A(t)\mu_A(1-q^i_B(t)) + p^i_S(t)(1-q^i_{AB}(t))f^i_B(t) \tag{S18c}$$

The different $q^i_x(t)$ denote the probability of node i not being infected by disease x by any of the simplices it participates to. Considering again only contributions up to $D = 2$, we have:

$$q^i_A(t) = \prod_{j\in\mathcal{V}} \Big\{1 - a_{ij}\epsilon_{BA}\beta_A[p^j_A(t) + p^j_{AB}(t)]\Big\} \prod_{j,l\in\mathcal{V}} \Big[1 - a_{ijl}\epsilon_{BA}\beta^{\triangle}_A[p^j_A(t) + p^j_{AB}(t)][p^l_A(t) + p^l_{AB}(t)]\Big] \tag{S19a}$$
$$q^i_B(t) = \prod_{j\in\mathcal{V}} \Big\{1 - a_{ij}\epsilon_{AB}\beta_B[p^j_B(t) + p^j_{AB}(t)]\Big\} \prod_{j,l\in\mathcal{V}} \Big[1 - a_{ijl}\epsilon_{AB}\beta^{\triangle}_B[p^j_B(t) + p^j_{AB}(t)][p^l_B(t) + p^l_{AB}(t)]\Big] \tag{S19b}$$
$$\begin{aligned} q^i_{AB}(t) = &\prod_{j\in\mathcal{V}} \Big\{1 - a_{ij}\Big[\beta_a[p^j_A(t) + p^j_{AB}(t)] + \beta_B[p^j_B(t) + p^j_{AB}(t)] - \beta_A\beta_B[p^j_{AB}(t)]^2\Big]\Big\} \\ &\prod_{j,l\in\mathcal{V}} \Big\{1 - a_{ijl}\Big[\beta^{\triangle}_A[p^j_A(t) + p^j_{AB}(t)][p^l_A(t) + p^l_{AB}(t)] + \beta^{\triangle}_B[p^j_B(t) + p^j_{AB}(t)][p^l_B(t) + p^l_{AB}(t)]\Big]\Big\} \end{aligned} \tag{S19c}$$

where the first product of each equation accounts for the contagion through the links of the simplicial complex $\mathcal{K}$. These links are fully specified by means of the standard adjacency matrix $\{a_{ij}\}$, whose elements $a_{ij} = 0, 1$ denote the absence or presence of a link (i, j). Similarly, the second product accounts for the contagion of i through the 2-simplices of $\mathcal{K}$ (triangles), which are

analogously specified by the elements of the adjacency tensor $\{a_{ijl}\}$. This tensor is the 3-dimensional version of the adjacency matrix, in which a non-zero element denotes the presence of a 2-simplex (i, j, l).

Finally, the factors $f_A^i(t)$ and $f_B^i(t)$ in Eq. (S18) denote the probability of transitioning from the status S to one of the states A or B when exposed simultaneously to both pathogens. Assuming equal probability for both diseases [37], we can write:

$$f_A^i(t) = \frac{\bar{q}_A^i(t)(1-0.5\bar{q}_B^i(t))}{\bar{q}_A^i(t)(1-\bar{q}_B^i(t)) + \bar{q}_B^i(t)(1-0.5\bar{q}_A^i(t))} \tag{S20a}$$

$$f_B^i(t) = \frac{\bar{q}_B^i(t)(1-0.5\bar{q}_A^i(t))}{\bar{q}_A^i(t)(1-\bar{q}_B^i(t)) + \bar{q}_B^i(t)(1-0.5\bar{q}_A^i(t))} \tag{S20b}$$

where $\bar{q}_A^i(t)$ and $\bar{q}_B^i(t)$ correspond to $1-q_A^i(t)$ and $1-q_B^i(t)$, as given by Eqs. (S19), after setting $\epsilon_{AB} = \epsilon_{BA} = 1$.

IV. CASE OF DIFFERENT RECOVERY RATES: $\mu_A \neq \mu_B$

In the main text we assumed identical recovery rates. Here, we remove this constraint and allow them to be potentially different, so that $\mu_A \neq \mu_B$. By rescaling all equations by μ_A (instead of μ), we have the following—instead of Eqs. (S3):

$$\dot{\rho}_A = -1\rho_A + \lambda_A\rho_S(\rho_A+\rho_{AB}) + \lambda_A^{\triangle}\rho_S(\rho_A+\rho_{AB})^2 + \frac{\mu_B}{\mu_A}\rho_{AB} - \epsilon_{AB}\lambda_B\frac{\mu_B}{\mu_A}\rho_A(\rho_B+\rho_{AB}) \tag{S21a}$$

$$\dot{\rho}_B = -\frac{\mu_B}{\mu_A}\rho_B + \lambda_B\frac{\mu_B}{\mu_A}\rho_S(\rho_B+\rho_{AB}) + 1\rho_{AB} - \lambda_A\rho_B(\rho_A+\rho_{AB}) - \lambda_A^{\triangle}\rho_B(\rho_A+\rho_{AB})^2 \tag{S21b}$$

$$\dot{\rho}_{AB} = -(1+\frac{\mu_B}{\mu_A})\rho_{AB} + \epsilon_{AB}\lambda_B\frac{\mu_B}{\mu_A}\rho_A(\rho_B+\rho_{AB}) + \lambda_A\rho_B(\rho_A+\rho_{AB}) + \lambda_A^{\triangle}\rho_B(\rho_A+\rho_{AB})^2 \tag{S21c}$$

which, introducing the total densities, becomes

$$\dot{\rho}_{A_{\text{tot}}} = (-\rho_A-\rho_{AB}) + \lambda_A\rho_{A_{\text{tot}}}[1-\rho_{B_{\text{tot}}}-\rho_A+\rho_B] + \lambda_A^{\triangle}\rho_{A_{\text{tot}}}^2[1-\rho_{B_{\text{tot}}}-\rho_A+\rho_B] \tag{S22a}$$

$$\dot{\rho}_{B_{\text{tot}}} = (-\rho_B-\rho_{AB})\frac{\mu_B}{\mu_A} + \lambda_B\frac{\mu_B}{\mu_A}\rho_{B_{\text{tot}}}[1-\rho_{A_{\text{tot}}}-\rho_B+\epsilon_{AB}\rho_A] \tag{S22b}$$

$$\dot{\rho}_{AB} = -(1+\frac{\mu_B}{\mu_A})\rho_{AB} + \epsilon_{AB}\lambda_B\frac{\mu_B}{\mu_A}\rho_A\rho_{B_{\text{tot}}} + \lambda_A\rho_B\rho_{A_{\text{tot}}} + \lambda_A^{\triangle}\rho_B\rho_{A_{\text{tot}}}^2. \tag{S22c}$$

and then

$$\dot{\rho}_{A_{\text{tot}}} = -\rho_{A_{\text{tot}}}1 + \lambda_A\rho_{A_{\text{tot}}}[1-\rho_{A_{\text{tot}}}] + \lambda_A^{\triangle}\rho_{A_{\text{tot}}}^2[1-\rho_{A_{\text{tot}}}] \tag{S23a}$$

$$\dot{\rho}_{B_{\text{tot}}} = -\rho_{B_{\text{tot}}}\frac{\mu_B}{\mu_A} + \lambda_B\frac{\mu_B}{\mu_A}\rho_{B_{\text{tot}}}[1-\rho_{A_{\text{tot}}}-\rho_{B_{\text{tot}}}+\rho_{AB}+\epsilon_{AB}(\rho_{A_{\text{tot}}}-\rho_{AB})] \tag{S23b}$$

$$\dot{\rho}_{AB} = -(1+\frac{\mu_B}{\mu_A})\rho_{AB} + \epsilon_{AB}\lambda_B\frac{\mu_B}{\mu_A}(\rho_{A_{\text{tot}}}-\rho_{AB})\rho_{B_{\text{tot}}} + \lambda_A(\rho_{B_{\text{tot}}}-\rho_{AB})\rho_{A_{\text{tot}}} + \lambda_A^{\triangle}(\rho_{B_{\text{tot}}}-\rho_{AB})\rho_{A_{\text{tot}}}^2 \tag{S23c}$$

which, compared to the case of identical recovery rates, contain the additional $\frac{\mu_B}{\mu_A}$ factors. We denote that dimensionless ratio $\delta = \frac{\mu_B}{\mu_A}$ and the equations become, after refactoring:

$$\dot{\rho}_{A_{\text{tot}}} = \rho_{A_{\text{tot}}}[-1+\lambda_A(1-\rho_{A_{\text{tot}}}) + \lambda_A^{\triangle}\rho_{A_{\text{tot}}}(1-\rho_{A_{\text{tot}}})], \tag{S24a}$$

$$\dot{\rho}_{B_{\text{tot}}} = \rho_{B_{\text{tot}}}\delta[-1+\lambda_B(1-\rho_{B_{\text{tot}}}) + \lambda_B(\epsilon_{AB}-1)(\rho_{A_{\text{tot}}}-\rho_{AB})], \tag{S24b}$$

$$\dot{\rho}_{AB} = -(1+\delta)\rho_{AB} + \epsilon_{AB}\lambda_B\delta(\rho_{A_{\text{tot}}}-\rho_{AB})\rho_{B_{\text{tot}}} + \lambda_A(\rho_{B_{\text{tot}}}-\rho_{AB})\rho_{A_{\text{tot}}} + \lambda_A^{\triangle}(\rho_{B_{\text{tot}}}-\rho_{AB})\rho_{A_{\text{tot}}}^2. \tag{S24c}$$

So, the equation for $\rho_{A_{\text{tot}}}$ (simplagion) is unchanged, as expected. For $\rho_{B_{\text{tot}}}$, we notice a temporal rescaling by a factor δ, but the implicit solution is unchanged,

$$\rho_{B_{\text{tot}}}^{*,\pm} = 1 - \frac{1}{\lambda_B} + (\rho_{A_{\text{tot}}}^{*,\pm} - \rho_{AB}^{*,\pm})(\epsilon_{AB}-1). \tag{S25}$$

We can consider two limits where the timescales for A and B are of different orders. First, in the limit $\delta \ll 1$, which means that B heals much slower than A, $\dot{\rho}_{B_{\text{tot}}} \approx 0$, that is process B is quasi-static compared to the timescale of process A. Thus, $\rho_{A_{\text{tot}}}$ converges fast to its NESS and $\rho_{B_{\text{tot}}}$ is driven by that NESS. Second, in the limit $\delta \gg 1$, B heals much faster than A, it is the opposite. It is possible then to rescale time by δ to see that process A now appears quasi-static compared to the timescale of B. So, $\rho_{B_{\text{tot}}}$ converges fast to its NESS which is in fact adiabatically moving towards its asymptotic NESS, driven by $\rho_{A_{\text{tot}}}$ that slowly converges to its own NESS.

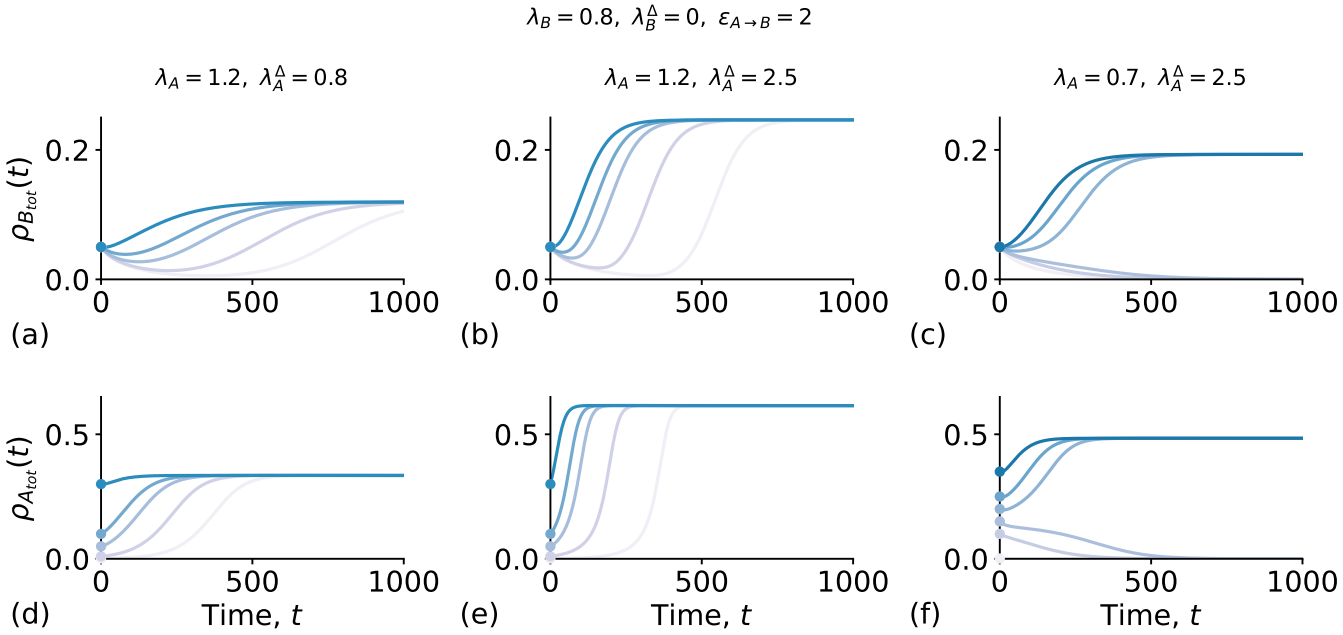

FIG. S1. The temporal evolution of the simple contagion B is affected by the initial conditions of the hidden driver process A. As for Fig. 5 of the main text, we show $\rho_{B_{\text{tot}}}$ over time (a-c), but together with the temporal dynamics of the driver process, as given by $\rho_{A_{\text{tot}}}$ (d-f). In (a,d) a simple driver process is used ($\lambda_A^{\triangle} = 0.8$), while in (b,e) and (c,f) the driver process A is truly simplicial ($\lambda_A^{\triangle} = 2.5$). The process A is placed either in the endemic region, $\lambda_A = 1.2$ [(a,d) and (b,e)] or in the bi-stable region ($\lambda_A = 0.7$). Different curves correspond to different initial conditions of the driver process, $\rho_A(0)$. The other parameters are set to $\lambda_B = 0.8$, $\lambda_B^{\triangle} = 0$, and $\epsilon_{AB} = 2$.

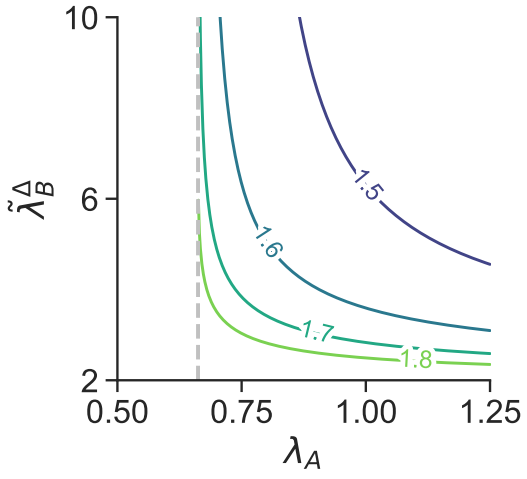

FIG. S2. Effective triangle infectivity $\tilde{\lambda}_B^{\triangle}$ of simple contagion B as a function of λ_A, for several values of the interaction ϵ_{AB} (indicated on the curves). The dashed grey curve indicates the value λ_A^c, where diverge $\tilde{\lambda}_B^{\triangle}$ diverges.

P07

Physics of Growth Regulation in Cells and Tissues

Jigyasa Watwani

International Centre for Theoretical Sciences,

Tata Institute of Fundamental Research.

It is necessary that biological systems stop growing after reaching a target size. Although significant insights have been gained by studying size regulation via morphogens in the wing disc of the fruit fly, *D. melanogaster*, we still do not fully understand the mechanical aspects of growth control and termination. Here, we present a framework to model growth in a 1-D tissue, where couplings between mechanics, growth and signaling arise naturally.

We model an isolated tissue as a continuum of cells. That is, at each point, we define relevant macroscopic fields – a displacement field of cells, a density field and concentration fields of signaling morphogens that tell the cells when to divide (Fig 1). The idea is to write

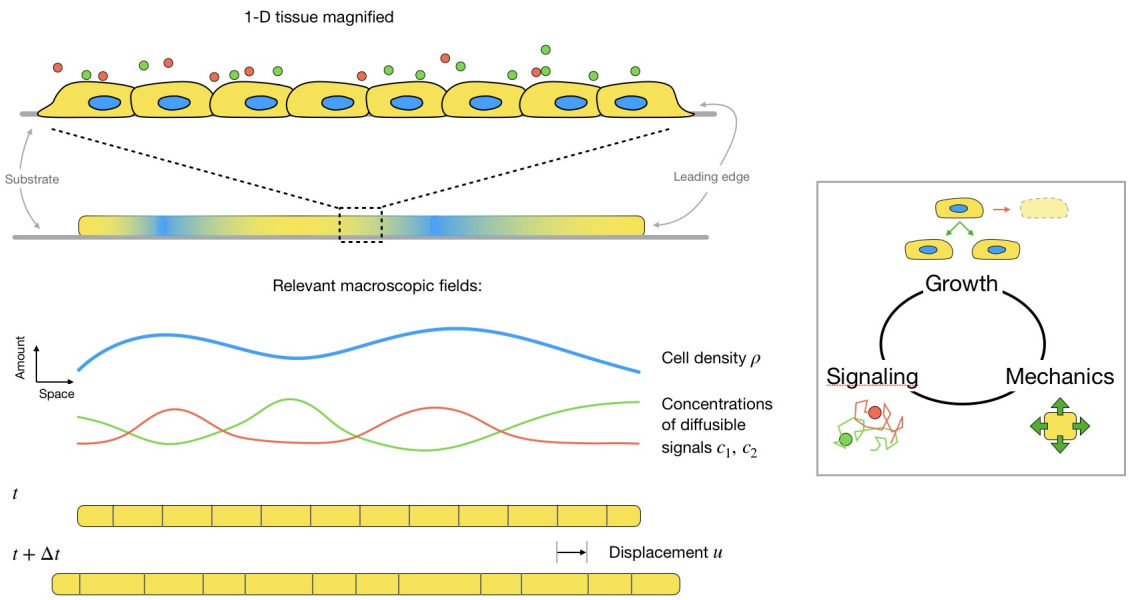

FIG. 1: Growth control in a 1-D tissue can be modeled by writing down hydrodynamic equations for the density of cells, displacement of cells and concentrations of signaling morphogens in the tissue.

hydrodynamic equations for the evolution of these fields on a growing domain and ask questions about the dynamics of growth up to a target size and mechanisms that stop growth beyond this target size.

We want to formulate the latter as a control problem – by demanding that the tissue passes through a given time sequence of steady state lengths $L^\star(t)$, we would like to reverse-engineer and extract out the minimal requirements for the model to to do so.